Segmentation Techniques for Iris Recognition System

Article

2 authors:

Surjeet Singh
The Jackson Laboratory

26 PUBLICATIONS   **239** CITATIONS

Kulbir Singh
Thapar Institute of Engineering and Technology

88 PUBLICATIONS   **1,113** CITATIONS

Some of the authors of this publication are also working on these related projects:

Project research paper View project

Project Mechanisms Underlying a Protective ApoE Variant in Alzheimer's Disease View project

Segmentation Techniques for Iris Recognition System

Surjeet Singh, Kulbir Singh

Abstract— A biometric system provides automatic identification of an individual based on a unique feature or characteristic possessed by the individual. Iris recognition is regarded as the most reliable and accurate biometric identification system available. Iris recognition systems capture an image of an individual's eye, the iris in the image is then segmented and normalized for feature extraction process. The performance of iris recognition systems highly depends on segmentation and normalization. This paper discusses the performance of segmentation techniques for iris recognition systems to increase the overall accuracy.

Index Terms—Active contour, Biometrics, Daugman's method, Hough Transform, Iris, Level Set method, Segmentation.

————————————— ◆ —————————————

1. INTRODUCTION

Reliable personal recognition is critical to many processes. Nowadays, modern societies give higher relevance to systems that contribute to the increase of security and reliability, essentially due to terrorism and other extremism or illegal acts. In this context, the use of biometric systems has been increasingly encouraged by public and private entities in order to replace or improve traditional security systems. Basically, the aim is to establish an identity based on who the person is, rather than on what the person possesses or what the person remembers.

Biometrics can be regarded as the automated measurement and enumeration of biological characteristics, in order to obtain a plausible quantitative value that, with high confidence, can distinguish between individuals.

Although less automatized, biometrics has been used - at least - for centuries. In the 14th century, the Portuguese writer João de Barros reported its first known application. He wrote that Chinese merchants stamped children's palm print and footprints on paper with identification purposes. In the western world, until the late 1800s the automatic recognition of individuals was largely done using "photographic memory". In 1883, the French police and anthropologist Alphonse Bertillon developed an anthropometric system, known as Bertillonage, to fix the problem of identification of convicted criminals.

In 1880, the British scientific journal Nature published an article by Henry Faulds and William James describing the uniqueness and permanence of fingerprints. This motivated the design of the first elementary fingerprint recognition system by Sir Francis Galton and improved by Sir Edward R. Henry. Having quickly disseminated, the first fingerprint system in the United States was inaugurated by the New York State Prison Department in 1903 and the first known convicted due to fingerprint evidences was reported in 1911.

Presently, due to increasing concerns associated with security and the war on terrorism, biometrics has considerably increased its relevance. It has moved from a single and almost standardized trait (fingerprint) to the use of more than ten distinct traits.

According to Matyas Jr. and Riha [1], every biometric system depends on the features, whether genotypic or phenotypic it is based on. Similarly to Daugman [2], authors divide the biometric traits into two types. Fried [3] and A. Bromba [4] classified the origin of the biometric traits into three different types: genotypic, behavioral, and randotypic.

Following the proposal of Jain et al. [5], biometric systems can be evaluated regarding seven parameters: uniqueness, universality, permanence, collectability, performance, acceptability and circumvention.

Figure 2 contains a comparison between the most common biometric traits. Each value was obtained through averaging and weighting of the classifications proposed in [6], [7], [4], [8], [9], [10] and [11].

For the purposes of our work, one of the most important features is the ability to perform

———————————————————

- *Surjeet Singh is currently faculty Member at Faculty of Science & Technology, The iCFAI University, Dehradun, Inida. E-mail: surjeet_singh1986@ymail.com*
- *Kulbir Singh is currenty Assistant Professor, in Electronics & Communication Engineering Department,Thapar University, Patiala, India. E-mail: ksingh@thapar.edu*

covert recognition, which can be performed by the fingerprint, face, iris and palmprint. Among these, iris must be enhanced, as it provides higher uniqueness and circumvention values.
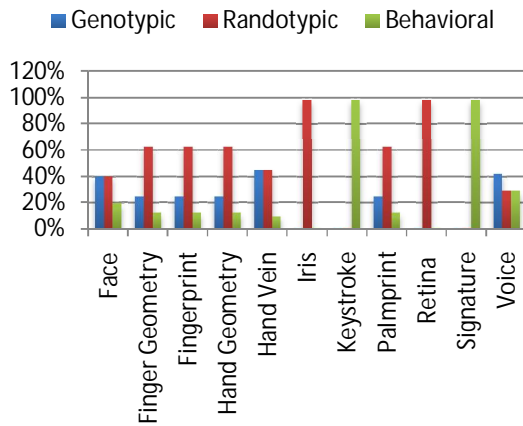

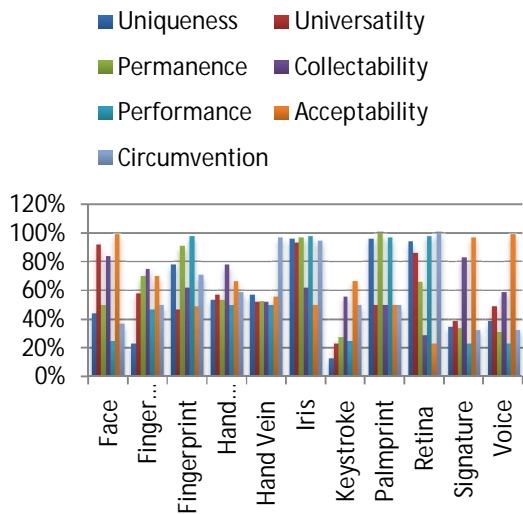Fig 1: Factors of influence of the biometric traits.

Fig 2: Comparison between the most common biometric traits (adapted and averaged from [6], [7], [4], [8], [9], [10] and [11]).

2. IRIS ANATOMY

The iris is a thin, circular structure located anterior to the lens, often compared to a diaphragm of an optical system. The centre aperture, the pupil, actually is located slightly nasal and inferior to the iris centre. Pupil size regulates retinal illumination. The diameter can vary from 1 mm to 9 mm depending on lighting conditions. The pupil is very small (miotic) in brightly lit conditions and fairly large (mydriatic) in dim illumination. The average diameter of the iris is 12 mm, and its thickness varies. It is thickest in the region of the collarette, a circular ridge approximately 1.5 mm from the pupillary margin. This slightly raised jagged ridge was the attachment site for the fetal pupillary membrane

during embryologic development. The collarette divides the iris into the pupillary zone, which encircles the pupil, and the ciliary zone, which extends from the collarette to the iris root. The colour of these two zones often differs [12].

The pupillary margin of the iris rests on the anterior surface of the lens and, in profile, the iris has a truncated cone shape such that the pupillary margin lies anterior to its peripheral termination, the iris root. The root, approximately 0.5 mm thick, is the thinnest part of the iris and joins the iris to the anterior aspect of the ciliary body. The iris divides the anterior segment of the globe into anterior and posterior chambers, and the pupil allows the aqueous humor to flow from the posterior into the anterior chamber with no resistance.
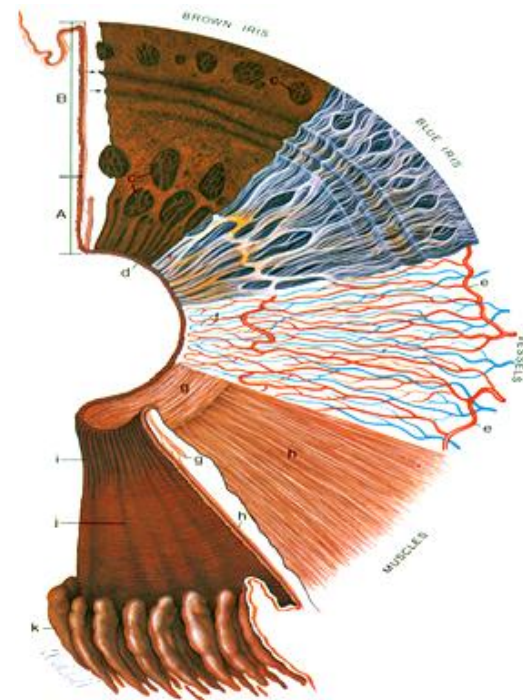

Fig 3: Surfaces and layers of the iris [12].

In figure 3 the iris cross-section shows the papillary (A) and ciliary portions (B), and the surface view shows a brown iris with its dense, matted anterior border layer. Circular contraction furrows are shown (arrows) in the ciliary portion of the iris. Fuchs' crypts (c) are seen at either side of the collarette in the pupillary and ciliary portion and peripherally near the iris root. The pigment ruff is seen at the pupillary edge (d). The blue iris surface shows a less dense anterior border layer and more prominent trabeculae. The iris vessels are shown beginning at the major arterial circle in the ciliary body (e). Radial branches of the arteries and veins extend toward the pupillary region. The arteries form the incomplete minor arterial circle

(f), from which branches extend toward the pupil, forming capillary arcades. The sector below it demonstrates the circular arrangement of the sphincter muscle (g) and the radial processes of the dilator muscle (h). The posterior surface of the iris shows the radial contraction furrows (i) and the structural folds of Schwalbe (j). Circular contraction folds also are present in the ciliary portion. The pars plicata of the ciliary body is at (k). [13]

3. IRIS SEGMENTATION

In this paper CASIA iris image database has been used for the analysis of different segmentation algorithms. CASIA iris image database (version 1.0) includes 756 iris images from 108 eyes, hence 108 classes.

In 1993, J. Daugman [14] presented one of the most relevant methods, constituting the basis of the majority of the functioning systems. Regarding the segmentation stage, this author introduced an integrodifferential operator to find both the iris inner and outer borders. This operator remains actual and was proposed in 2004 with minor differences by Nishino and Nayar [15].

Similarly, Camus and Wildes [16] and Martin-Roche et al. [17] proposed integrodifferential operators that search the $\mathbb{N}^3$ space, with the objective of maximizing the equations that identify the iris borders.

Wildes [18] proposed iris segmentation through a gradient based binary edge-map construction followed by circular Hough transform. This is the most common method, that has been proposed with minor variants by Cui et al. [19], Huang et al.[20], Kong and Zhang[21], Ma et al.[22], [23] and [24].

Liam et al. [25] proposed one interesting method essentially due to its simplicity. This method is based in thresholds and in the maximization of a simple function, in order to obtain two ring parameters that correspond to iris inner and outer borders.

Du et al. [26] proposed the iris detection method based on the prior pupil segmentation. The image is further transformed into polar coordinates and the iris outer border is detected as the largest horizontal edge resultant from Sobel filtering. However, this approach may fail in case of non-concentric iris and pupil, as well as for very dark iris textures.

Morphologic operators were applied by Mira and Mayer [27] to obtain iris borders. They detected the pupillary and scleric borders by applying thresholding, image opening and closing.

Based on the assumption that the pixels' intensity of the captured image can be well represented by a mixture of three Gaussian distributions, Kim et al. [28] proposed the use of Expectation Maximization [29] algorithm to estimate the respective distribution parameters. They expected that 'Dark', 'Intermediate' and 'Bright' distributions contain the pixels corresponding to the pupil, iris and reflections areas.

3.1 Daugman's Method

This is by far the most cited method [14] in the iris recognition literature. The author assumes both pupil and iris with circular form and applies the following integrodifferential operator:

$$\max_{r, x_0, y_0} \left| G_\sigma(r) * \frac{\delta}{\delta r} \oint_{r, x_0, y_0} \frac{I(x,y)}{2\pi r} ds \right| \quad (1)$$

This operator searches over the image domain (x,y) for the maximum in the blurred (by a Gaussian Kernel $G_\sigma(r)$ partial derivative with respect to increasing radius r, of the normalized contour integral of $I(x,y)$ along a circular arc ds of radius r and center coordinates (x_0, y_0). In other words, this method searches in the $\mathbb{N}^3$ space for the circumference center and radius with highest derivative values comparing to circumferences of neighbour radius.

At first the blurring factor σ is set for a coarse scale of analysis so that only the very pronounced circular transition from iris to (white) sclera is detected. Then after this strong circular boundary is more precisely estimated, a second search begins within the confined central interior of the located iris for the fainter pupillary boundary, using a finer convolution scale σ and a smaller search range defining the paths (x_0, y_0, r) contour integration. In the initial search for the outer bounds of the iris, the angular arc of contour integration ds is restricted in range to two opposing 90^0 cones centered on the horizontal meridian, since eyelids generally obscure the upper and lower limbus of the iris. Then in the subsequent interior search for the pupillary boundary, the arc of contour integration ds in operator (1) is restricted to the upper 270^0 in order to avoid the corneal specular reflection that is usually superimposed in the lower 90^0 cone of the iris from the illuminator located below the video camera. Taking the absolute value in (1) is not required when the operator is used first to locate the outer boundary of the iris, since the sclera is always lighter than the iris and so the smoothed partial derivative with increasing radius near the limbus is always positive. However, the pupil is not always darker than the iris, as in persons with normal early cataract or significant back-

scattered light from the lens and vitreous humor; applying the absolute value in **(1)** makes the operator a good circular edge-finder regardless of such polarity-reversing conditions. With σ automatically tailored to the stage of search for both the pupil and limbus, and by making it correspondingly finer in successive iterations, the operator defined in **(1)** has proven to be virtually infallible in locating the visible inner and outer annular boundaries of irises.
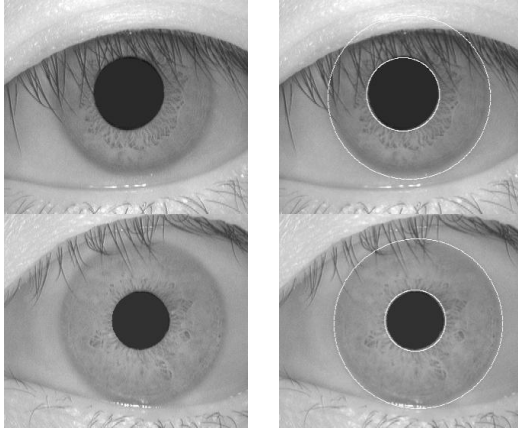

Fig 4: Segmentation by Daugman's Method

For rapid discrete implementation of the integrodifferential operator in **(1)**, it is more efficient to interchange the order of convolution and differentiation and to concatenate them, before computing the discrete convolution of the resulting operator with the discrete series of undersampled sums of pixels along circular contours of increasing radius. Using the finite difference approximation to the derivative for a discrete series in **n**,

$$\frac{\partial \mathbf{G}_\sigma(\mathbf{r})}{\partial \mathbf{r}} \approx \mathbf{G}^1_\sigma(\mathbf{n}) = \frac{1}{\Delta \mathbf{r}} \mathbf{G}_\sigma(n\Delta \mathbf{r})$$
$$- \frac{1}{\Delta \mathbf{r}} \mathbf{G}_\sigma\big((n-\mathbf{1})\Delta \mathbf{r}\big) \quad \mathbf{(2)}$$

where Δ**r** is a small increment in radius, and replacing the convolution and contour integrals with sums, we can derive through these manipulations an efficient discrete operator (3) for finding the inner and outer boundaries of an iris where Δθ is the angular sampling interval along the circular arcs, over which the summed **I (x ,y)** pixel intensities represent the contour integrals expressed in **(1)**.

3.2 Hough Transform

Hough transform is a standard image analysis tool for finding curves that can be defined in a parametrical form such as lines, polynomials and circles. The recognition of a global pattern is achieved using the local patterns. For instance, recognition of a circle can be achieved by considering the strong edges in an image as the local patterns and searching for the maximum value of a circular Hough transform.

Wildes et al. [18], Kong and Zhang [21], Tisse et al. [30] and Ma et al. [22] use Hough transform to localize irises. The localization method, similar to Daugman's method, is also based on the first derivative of the image. In the proposed method by Wildes, an edge map of the image is first obtained by thresholding the magnitude of the image intensity gradient:

$$|\nabla \mathbf{G(x,y)} * \mathbf{I(x,y)}| \qquad \mathbf{(3)}$$

Where $\nabla \equiv (\partial/\partial \mathbf{x}, \partial/\partial \mathbf{y})$ and $\mathbf{G(x,y)} = \frac{1}{2\pi\sigma^2}\mathbf{e}^{-\frac{(x-x_0)^2+(y-y_0)^2}{2\sigma^2}}$. **G(x,y)** is a Gaussian smoothing function with scaling parameter σ to select the proper scale of edge analysis.

The edge map is then used in a voting process to maximize the defined Hough transform for the desired contour. Considering the obtained edge points as $(\mathbf{x_j ,y_j}), \mathbf{j = 1,2,\dots,n}$, a Hough transform can be written as:

$$\mathbf{H(x_c,y_c,r)} = \sum_{j=1}^{n} h\big(\mathbf{x_j,y_j,x_c,y_c,r}\big) \qquad \mathbf{(4)}$$

where

$$h\big(\mathbf{x_j,y_j,x_c,y_c,r}\big) =$$
$$\begin{cases} \mathbf{1 \ if \ g(x_j,y_j,x_c,y_c,r) = 0} \\ \mathbf{0 \ otherwise} \end{cases} \qquad 5)$$

The limbus and pupil are both modeled as circles and the parametric function **g** is defined as:

$$\mathbf{g(x_j,y_j,x_c,y_c,r)} = \big(\mathbf{x_j} - \mathbf{x_c}\big)^2 + \big(\mathbf{y_j} - \mathbf{y_c}\big)^2$$
$$- \mathbf{r}^2 \qquad \mathbf{(6)}$$

Assuming a circle with the center **(x_c,y_c)** and radius **r**, the edge points that are located over the circle result in a zero value of the function. The value of **g** is then transformed to **1** by the h function, which represents the local pattern of the contour. The local patterns are then used in a voting procedure using the Hough transform, **H**, in order to locate the proper pupil and limbus boundaries. In order to detect limbus, only vertical edge information is used. The upper and lower parts, which have the horizontal edge information, are usually covered by the two eyelids. The horizontal edge information is used for detecting the upper and lower eyelids, which are modeled as parabolic arcs.

We implemented this method in MATLAB® by first employing Canny edge detection to generate an edge map. Gradients were biased in the vertical direction for the outer iris/sclera boundary, as suggested by Wildes et al. [24]. Vertical and horizontal gradients were weighted equally for the inner iris/pupil boundary.

The range of radius values to search for was set manually, depending on the database used. For the CASIA database, values of the iris radius range from 90 to 150 pixels, while the pupil radius ranges from 28 to 75 pixels. In order to make the circle detection process more efficient and accurate, the Hough transform for the

iris/sclera boundary was performed first, then the Hough transform for the iris/pupil boundary was performed within the iris region, instead of the whole eye region, since the pupil is always within the iris region.
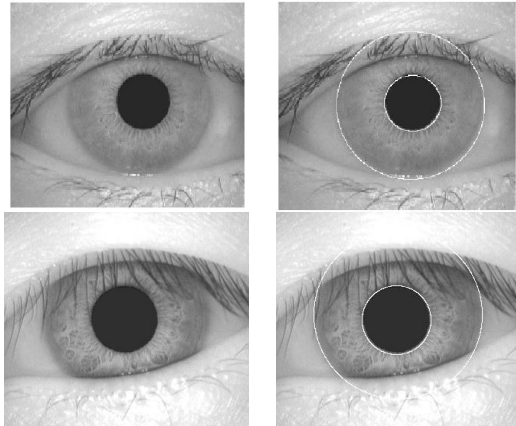

Fig 5: Segmentation by Hough Transform.

3.3 Variational Level Set Formulation of Active Contours without Re-initialization

In image segmentation, active contours are dynamic curves that moves toward the object boundaries. To achieve this goal, we explicitly define an external energy that can move the zero level curve toward the object boundaries. Let **I** be an image, and **g** be the edge indicator function defined

$$g = \frac{1}{1 + |\nabla G_\sigma * I|^2} \qquad (7)$$

where G_σ is the Gaussian kernel with standard deviation σ. We define an external energy for a function ϕ**(x, y)** as below

$$\mathcal{E}_{g,\lambda,\nu}(\phi) = \lambda \mathcal{L}_g(\phi) + \nu A_g(\phi) \qquad (8)$$

where λ **> 0** and ν are constants, and the terms $\mathcal{L}_g(\phi)$ and $A_g(\phi)$ are defined by

$$\mathcal{L}_g(\phi) = \int_\Omega g\delta(\phi)|\nabla\phi| dx dy$$

$$A_g(\phi) = \int_\Omega gH(-\phi) dx dy \qquad (9)$$

respectively, where δ is the univariate Dirac function, and **H** is the Heaviside function. Now, we define the following total energy functional

$$\mathcal{E}(\phi) = \mu P(\phi) + \mathcal{E}_{g,\lambda,\nu}(\phi) \qquad (10)$$

The external energy $\mathcal{E}_{g,\lambda,\nu}$ drives the zero level set toward the object boundaries, while the internal energy μ**P(ϕ)** penalizes the deviation of ϕ from a signed distance function during its evolution. To understand the geometric meaning of the energy, $\mathcal{L}_g(\phi)$ we suppose that the zero level set of ϕ can be represented by a differentiable parameterized curve **C(p)**, **p** ∈ **[0,1]**. It is well known that the energy functional $\mathcal{L}_g(\phi)$) computes the length of the zero level curve of ϕ in the conformal metric **ds** = **g(C(p))|C'(p)| dp**. The energy functional $A_g(\phi)$ in **(3.24)** is introduced to speed

up curve evolution. Note that, when the function **g** is constant **1**, the energy functional in **(9)** is the area of the region $\Omega_\phi^- = \{(x,y)|\phi(x,y) < 0\}$. The energy functional $A_g(\phi)$ in **(9)** can be viewed as the weighted area of Ω_ϕ^-. The coefficient ν of A_g can be positive or negative, depending on the relative position of the initial contour to the object of interest. For example, if the initial contours are placed outside the object, the coefficient ν in the weighted area term should take positive value, so that the contours can shrink faster. If the initial contours are placed inside the object, the coefficient ν should take negative value to speed up the expansion of the contours.

By calculus of variations , the Gateaux derivative (first variation) of the functional $\mathcal{E}$ in **(10)** can be written as

$$\frac{\partial \mathcal{E}}{\partial \phi} = -\mu\left[\Delta\phi - div\left(\frac{\nabla\phi}{|\nabla\phi|}\right)\right]$$

$$-\lambda\delta(\phi)div(g\frac{\nabla\phi}{|\nabla\phi|} - \nu g\delta(\phi) \qquad (11)$$

where Δ is the Laplacian operator. Therefore, the function ϕ that minimizes this functional satisfies the Euler-Lagrange equation $\frac{\partial \mathcal{E}}{\partial \phi} = 0$. The steepest descent process for minimization of the functional $\mathcal{E}$ is the following gradient flow:

$$\frac{\partial \phi}{\partial t} = \mu\left[\Delta\phi - div\left(\frac{\nabla\phi}{|\nabla\phi|}\right)\right]$$

$$-\lambda\delta(\phi)div(g\frac{\nabla\phi}{|\nabla\phi|} - \nu g\delta(\phi) \qquad (12)$$

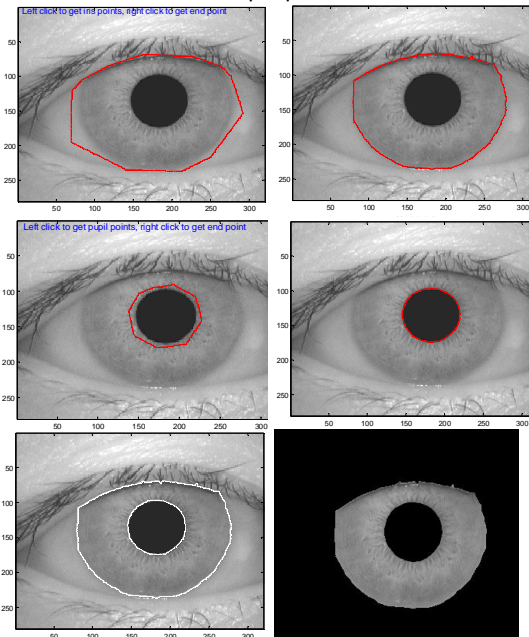this gradient flow is the evolution equation of the level set function in the proposed method.

Fig 6: (a) Selected iris mask (b) iris/sclera boundary (c) selected pupil mask (d) iris/pupil boundary (e) segmented image (f) iris region.

The second and the third term in the right hand side of **(12)** correspond to the gradient flows of the energy functional $\mathcal{L}_g(\phi)$ and $\nu\mathbf{A}_g(\phi)$, respectively, and are responsible of driving the zero level curve towards the object boundaries. To explain the effect of the first term, which is associated to the internal energy $\mu\mathbf{P}(\phi)$, we notice that the gradient flow

$$\Delta\phi - \mathbf{div}\left(\frac{\nabla\phi}{|\nabla\phi|}\right)$$
$$= \mathbf{div}\left[\left(1 - \frac{1}{|\nabla\phi|}\right)\nabla\phi\right] \qquad \textbf{(13)}$$

has the factor $\left(1 - \frac{1}{|\nabla\phi|}\right)$ as diffusion rate. If $|\nabla\phi| > 1$, the diffusion rate is positive and the effect of this term is the usual diffusion, i.e. making ϕ more even and therefore reduce the gradient $|\nabla\phi|$. If $|\nabla\phi| < 1$, the term has effect of reverse diffusion and therefore increase the gradient [31].

4. RESULTS

The automatic segmentation model using Integrodifferential equations and Hough transform proved to be successful. The CASIA database provided good segmentation, since those eye images had been taken specifically for iris recognition research and boundaries of iris pupil and sclera were clearly distinguished. For the CASIA database, the Hough transform based segmentation technique managed to correctly segment the iris region from 658 out of 756 eye images, which corresponds to a success rate of around 87% as compared to the Hough transform based segmentation technique that managed to correctly segment the iris region from 624 out of 756 eye images, which corresponds to a success rate of around 83%.

Using Integrodifferential equations and Hough transform methods on locating the pupil and limbus assume that the boundaries are perfect circles. Although the approaches are different, all these methods consider pupil and limbus as circular curves. It has been noticed that the circular assumption of the contours can lead to inappropriate boundary detection Figure 7 and 8.

The above methods of segmentation resulted in false detection due to noises such as strong boundaries of upper and lower eyelids. The strong eyelid boundaries and presence of eyelashes affected the limbus localization significantly.

We also implemented eyelashes and eyelids detection for the above two methods. The eyelid detection system proved quite successful, and managed to isolate most occluding eyelid regions. One problem was that it would sometimes isolate too much of the iris region,

which could make the recognition process less accurate, since there is less iris information. However, this is preferred over including too much of the iris region, if there is a high chance it would also include undetected eyelash and eyelid regions.
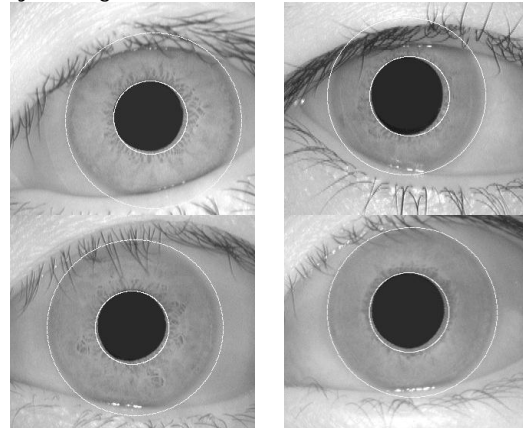
Fig 7: Illustrate the results of the Integrodifferential operator over the pupils that are not perfect circles. The circular contour does not detect pupil boundaries accurately.
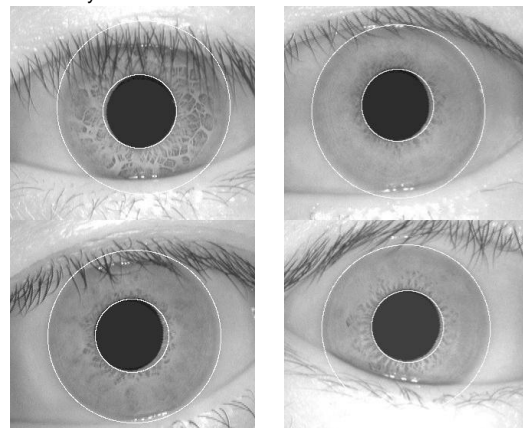
Fig 8: Illustrate the results of the Hough transform operator over the pupils that are not perfect circles. The circular contour does not detect pupil boundaries accurately.
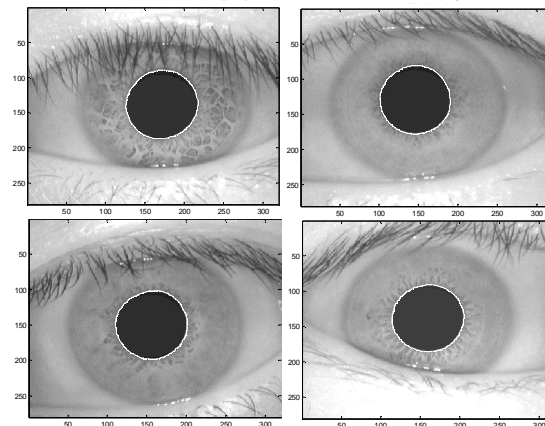
Fig 9: Illustrate the results of the active contour segmentation method based on Level set evolution without re-initialization over the pupils that are not perfect circles.

The eyelash detection system implemented for the CASIA database also proved to be successful in isolating most of the eyelashes occurring within the iris region as shown in Figure 11. A slight problem was that areas where the eyelashes were light, such as at the tips were not detected. However, these undetected areas were small when compared with the size of the iris region.
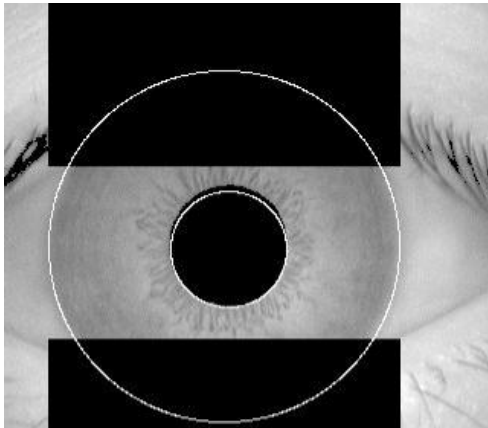

Fig 10: Automatic segmentation of image from CASIA database. Black region denote detected eyelid.
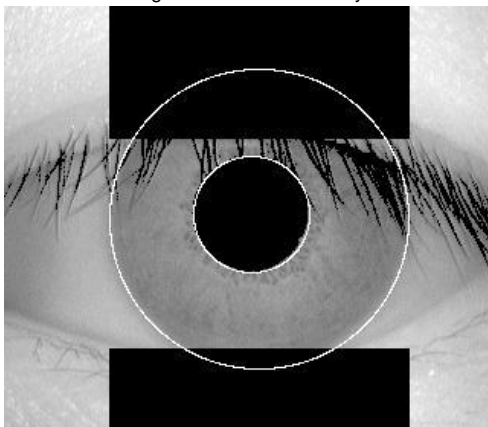

Fig 11: The eyelash detection technique, eyelash regions are detected using thresholding and denoted as black.

TABLE I

COMPARISON OF DIFFERENT SEGMENTATION TECHNIQUES.

Method	No. Of eye images	Properly Segmented	Accuracy
Daugman's Method	756	658	87%
Hough Transform	756	624	83%
Proposed Method	756	750	Approx: 100%

The proposed method of active contour segmentation based on Level set evolution without re-initialization provided perfect segmentation results for the pupil and limbus boundaries with success rate of almost 100%. Only problem with this system was that the initial contour was to be defined for each eye image manually.

REFERENCES

[1] V. Matyas and Z. Riha, "Toward reliable user authentication through biometrics," IEEE Security and Privacy, vol. 1, no. 3, pp. 45–49, 2003.

[2] J. G. Daugman, "Phenotypic versus genotypic approaches to face recognition," Face Recognition: From Theory to Applications, pp. 108–123. Heidelberg: Springer-Verlag, 1998.

[3] S. D. Fried, "Domain access control systems and methodology,"http://www.itu.dk/courses/SIAS/E2005/AU22 40 01.pdf , 2004.

[4] M. Bromba, Biometrics FAQ's, http://www.bromba.com/faq/biofaqe.htm, 2010.

[5] A. K. Jain, R. Bolle, and S. Pankanti, Personal Identification in networked society, 2nd edition. Kluwer Academic Publisher, E.U.A., 1999.

[6] A. K. Jain, A.Ross, and S. Prabhakar, "An introduction to biometric recognition," IEEE Transactions on Circuits and Systems for Video Technology, vol. 14, no. 1, pp. 4–19, January 2004.

[7] S. Liu and M. Silverman, "A practical guide to biometric security technology," IT Professional, vol. 3, no 1, pp. 27–32, January 2001.

[8] Biometrics and the courts, http://ctl.ncsc.dni.us/biomet%20web/BMIndex.html, 2010.

[9] Idesia's Biometric Technologies. Biometric comparison table,http://www.idesia-biometrics.com/technology/biometric_comparison_table. html, 2010.

[10] International Biometric Group, "Which is the best biometric technology?," http://www.biometricgroup.com/reports/public/report s/best_biometric.html, 2010.

[11] J. D. Woodward, K. W. Webb, E. M. Newton, M. A. Bradley, D. Rubenson, K. Larson, J. Lilly, K. Smythe, B. Houghton, H. A. Pincus, J. Schachter, and P. Steinberg, "Army Biometric Applications - Identifying and Addressing Socio-Cultural Concerns," Rand Corporation, Santa Monica, 2001.

[12] A. K. Khurana, Comprehensive Ophthalmology, New Age International (P) Ltd., 4th edition, 2007.

[13] L. A. Remington, Clinical Anatomy of the Visual System, Elsevier Inc., 2nd edition, 2005.

[14] J. G. Daugman, "High confidence visual recognition of persons by a test of statistical independence," IEEE Transactions on Pattern Analysis and Machine Intelligence, vol. 25, no. 11, pp. 1148–1161, November 1993.

[15] K. Nishino and S. K. Nayar, "Eyes for relighting," ACM Trans. Graph., vol 23, no. 3, pp. 704–711, 2004.

[16] T.A. Camus and R. Wildes, "Reliable and fast eye finding in close-up images," Proceedings of the IEEE 16th

International Conference on Pattern Recognition, pp. 389–394, Quebec, August 2002.

[17] D. Martin-Roche, C. Sanchez-Avila, and R. Sanchez-Reillo, "Iris recognition for biometric identification using dyadic wavelet transform zero-crossing," IEEE Aerospace and Electronic Systems Magazine, Mag. 17, no. 10, pp. 3–6, 2002.

[18] R. P. Wildes, "Iris recognition: an emerging biometric technology," Proceedings of the IEEE, vol. 85, no.9, pp. 1348–1363, U.S.A., September 1997.

[19] J. Cui, Y. Wang, T. Tan, L. Ma, and Z. Sun, "A fast and robust iris localization method based on texture segmentation," Proceedings of the SPIE Defense and Security Symposium, vol. 5404, pp. 401–408, August 2004.

[20] J. Huang, Y. Wang, T. Tan, and J. Cui, "A new iris segmentation method for recognition," Proceedings of the 17th International Conference on Pattern Recognition (ICPR), vol. 3, pp. 23–26, 2004.

[21] W. K. Kong and D. Zhang, "Accurate iris segmentation method based on novel reflection and eyelash detection model," Proceedings of the International Symposium on Intelligent Multimedia, Video and Speech Processing, pp. 263–266, Hong Kong, May 2001.

[22] L. Ma, Y. Wang, and T. Tan, "Iris recognition using circular symmetric filters," Proceedings of the 25th International Conference on Pattern Recognition, vol. 2, pp. 414–417, Quebec, August 2002.

[23] L. Ma, T. Tan, Y. Wang, and D. Zhang, "Personal identification based on iris texture analysis," IEEE Transactions on Pattern Analysis and Machine Intelligence, vol. 25, no. 12, pp. 2519–2533, December 2003.

[24] L. Ma, Y. Wang, and D. Zhang, "Efficient iris recognition by characterizing key local variations," IEEE Transactions on Image Processing, vol. 13, no. 6, pp. 739–750, June 2004.

[25] L. Liam, A. Chekima, L. Fan, and J. Dargham, "Iris recognition using self organizing neural network," Proceedings of the IEEE Student Conference on Research and Developing Systems, pp. 169–172, Malasya, June 2002.

[26] Y. Du, R. Ives, D. Etter, T. Welch, and C. Chang, "A new approach to iris pattern recognition," Proceedings of the SPIE European Symposium on Optics/Photonics in Defence and Security, vol. 5612, pp. 104–116, October 2004.

[27] J. Mira and J. Mayer, "Image feature extraction for application of biometric identification of iris - a morphological approach," Proceedings of the 16th Brazilian Symposium on Computer Graphics and Image Processing, pp. 391–398, Brazil, October 2003.

[28] J. Kim, S. Cho, and J. Choi, "Iris recognition using wavelet features," Kluwer Academic Publishers, Journal of VLSI Signal Processing, no. 38, pp. 147– 256, November 2004.

[29] A. P. Dempster, N. Laird, and D. Rubin, "Maximum likelyhood from incomplete data via the EM algorithm," Journal of the Royal Statistic Society, vol. 39, pp. 1–38, 1977.

[30] C. Tisse, L. Martin, L. Torres, and M. Robert, "Person identification technique using human iris recognition,"

Proceedings of the 25th International Conference on Vision Interface, pp. 294–299, Calgary, July 2002.

[31] C. Li, C. Xu, C. Gui, and M. D. Fox, "Level Set Evolution Without Re-initialization: A New Variational Formulation," IEEE Computer Society Conference on Computer Vision and Pattern Recognition, vol. 1, pp. 430 – 436, 2005.